

Mode-selective scattering of phonons in a semi-insulating GaAs crystal: A case study using phonon imaging

M. T. Ramsbey*

Department of Physics and Materials Research Laboratory, University of Illinois at Urbana-Champaign, Urbana, Illinois 61801

S. Tamura

Department of Engineering Science, Hokkaido University, Sapporo 060, Japan

J. P. Wolfe

Department of Physics and Materials Research Laboratory, University of Illinois at Urbana-Champaign, Urbana, Illinois 61801

(Received 25 October 1991)

Using a slotted-crystal geometry, phonon-imaging techniques, and Monte Carlo simulations, we have measured the absolute scattering rates of longitudinal and transverse phonons with frequency higher than 0.7 THz in undoped GaAs at $T=1.6$ K. Comparisons are made to the theoretical rate constant, $A_0=7.38\times 10^{-42}$ s³, for mass-defect scattering from naturally occurring isotopes in GaAs. The scattering of longitudinal phonons is found to be consistent with isotope scattering with the rate constant $A_L\leq 1.3A_0$; however, the transverse-phonon scattering is much stronger, yielding the rate constant $A_T=(4.0\pm 0.7)A_0$. This mode-selective scattering is inconsistent with simple elastic scattering from mass defects.

I. INTRODUCTION

With the advent of heat-pulse techniques,¹ it has become possible to observe the ballistic propagation of high-frequency acoustic phonons across crystals of macroscopic dimensions. These methods present the opportunity to make quantitative measurements of the scattering of phonons from defects in the limit of very few scattering events. This potential has not been realized in practice until recently, in large part because the ballistic phonon propagation is extremely anisotropic, and a determination of scattering rates requires a detailed accounting of this intrinsic elastic anisotropy. In addition, the scattering of phonons from defects in the crystal is known to be highly anisotropic, that is, dependent on the directions of the wave vectors and polarizations of incident and scattered phonons.²⁻⁵ On the experimental side, a clear separation of ballistic and scattered phonons is often not possible: the simplistic idea that scattered phonons can be isolated by their longer time of flight across the sample is complicated by a finite lifetime of the heat source⁶⁻¹⁰ and, in some cases, by dispersive phonon propagation.¹¹⁻¹³

Nevertheless, taking these factors into account, several attempts have been made to measure the scattering rates of high-frequency phonons in the semiconductors GaAs and silicon. In all cases, the anisotropic propagation is experimentally characterized by phonon imaging,¹⁴ and the calibration of scattering rates is extracted by theoretical modeling which, to varying degrees, includes the effects of elastic anisotropy. Phonon imaging permits the experimenter to accurately select a particular propagation direction of the ballistic phonons, and to identify phonons of particular polarization by their spatial and

temporal signatures. For GaAs, Held, Klein, and Huebener¹⁵ devised a procedure to extract the diffusive background from the sharp phonon-focusing structures associated with ballistic phonons. They deduced phonon mean free paths for wafers with varying densities of Cr impurities and dislocations. Fieseler, Wenderoth, and Ulbrich¹⁶ used a similar technique—as well as an analysis of the temporal pulse shapes¹⁷—to estimate the absolute scattering rate in an undoped-GaAs crystal. With phonon detection above 0.65 THz, they found a scattering rate comparable to that predicted from the naturally occurring isotopes, i.e., mass-defect scattering. Finally, Shields, Tamura, and Wolfe¹⁸ and Tamura, Shields, and Wolfe¹⁹ employed a slotted-crystal geometry,²⁰ combined with detailed Monte Carlo simulations, to measure the scattering rate of phonons in ultrapure silicon. Their analysis yielded a scattering rate which was within about 10% of that predicted for isotope scattering in silicon.

In the present paper, we apply the slotted-crystal technique to measure the scattering of high-frequency acoustic phonons in an undoped-GaAs crystal. Despite our expectations that the measured rate would be close to that predicted by isotope-scattering theory, we have found some interesting contrasts to the aforementioned studies of silicon.^{18,19} In particular, the scattering of transverse phonons is significantly higher than expected for a pure crystal, whereas the longitudinal phonon scattering is consistent with isotopes being the sole scattering centers. This differential scattering of longitudinal and transverse phonons implies the existence of additional scattering from residual defects in the crystal.

Several previous studies have observed the polarization-dependent scattering of phonons from defects in GaAs. From heat-pulse measurements along

high-symmetry axes, Narayanamurti, Chin, and Logan^{2,3} extracted the symmetry of Cr and DX centers. Similarly, Culbertson *et al.*²¹ observed a polarization-dependent scattering in undoped GaAs which was diminished after the application of infrared radiation. Their results were interpreted in terms of the so-called EL2 defect—believed to be an arsenic on a gallium site with a nearby impurity or interstitial—which has been associated with photoinduced metastability effects.²² Our present results may well be due to this defect in GaAs, which is naturally formed by the liquid-encapsulated-Czochralski (LEC) growth method for semi-insulating GaAs.

II. EXPERIMENTAL MEASUREMENTS AND ANALYSIS

The essential aspects of our experiments are shown in Fig. 1. We employed an undoped crystal of GaAs grown by the LEC method by Wacker Chemitronics.²³ The crystal was cut into a parallelepiped with large faces normal to [110], and these faces were polished with alumina and finally with SYTON colloidal-silica solution. A slot was cut in the crystal with a wire coated with an abrasive slurry, as shown in Fig. 1(a). The final stages of the cut were made with very little pressure on the wire to minimize subsurface damage. A 2000-Å copper film was deposited on one of the large surfaces; excitation of this surface with a focused laser beam provided a small (10 μm in diameter) movable heat source. A $5 \times 17 \mu\text{m}^2$ Pb-Bi tunnel junction was deposited on the opposite face, as shown in the figure. The onset frequency of this detector was measured to be 0.7 THz from its I - V characteristic. The sample was immersed in liquid helium, vacuum pumped to a temperature of 1.6 K.

Figure 1(b) shows a schematic of the phonon caustic pattern for (110) excitation of GaAs. The heavy vertical line indicates the boundary of the slot. For laser-spot positions to the right of this boundary, we expect to observe both ballistic and scattered phonons, whereas for positions to the left of the boundary, only scattered phonons can be detected. A boxcar averager is used to select a range of propagation times after the 15-ns laser pulse (from a cavity-dumped Ar⁺ laser with $\lambda \approx 5000$ Å). Typically, we choose an observation window between t_b and $1.5t_b$, where t_b is the ballistic time of flight of phonons (longitudinal or transverse) along the [100] axis. The cutoff at $1.5t_b$ eliminates the possibility of detecting phonons scattered from the side surfaces of the crystal. A "line scan" of the phonon intensity, as defined in Fig. 1(b), is plotted as the solid line in Fig. 1(c). The signals to the left of the slot boundary are greatly reduced because the slot prevents the detection of ballistic phonons in this region. A significant flux of scattered phonons, however, is observed to the left of the boundary. We show as the dashed line the probable signal if there were no slot in the sample, as obtained by reflecting the signal at the right about $\theta=0^\circ$. An alternative measurement is the "bar scan" in which phonon intensity is integrated over a vertical "bar" defined as a single image column within the shaded area of Fig. 1(b).

Figure 2 shows the complete phonon images of this

crystal obtained by selecting either longitudinal or transverse times of flight. The longitudinal pattern shows significant concentrations of ballistic flux along the $\langle 110 \rangle$ and $\langle 111 \rangle$ directions (no caustics are predicted for longitudinal phonons in the present experimental frequency regime¹⁴). The slot boundary at the left marks a great reduction in phonon flux. The transverse pattern displays the expected caustics, although intensity in the

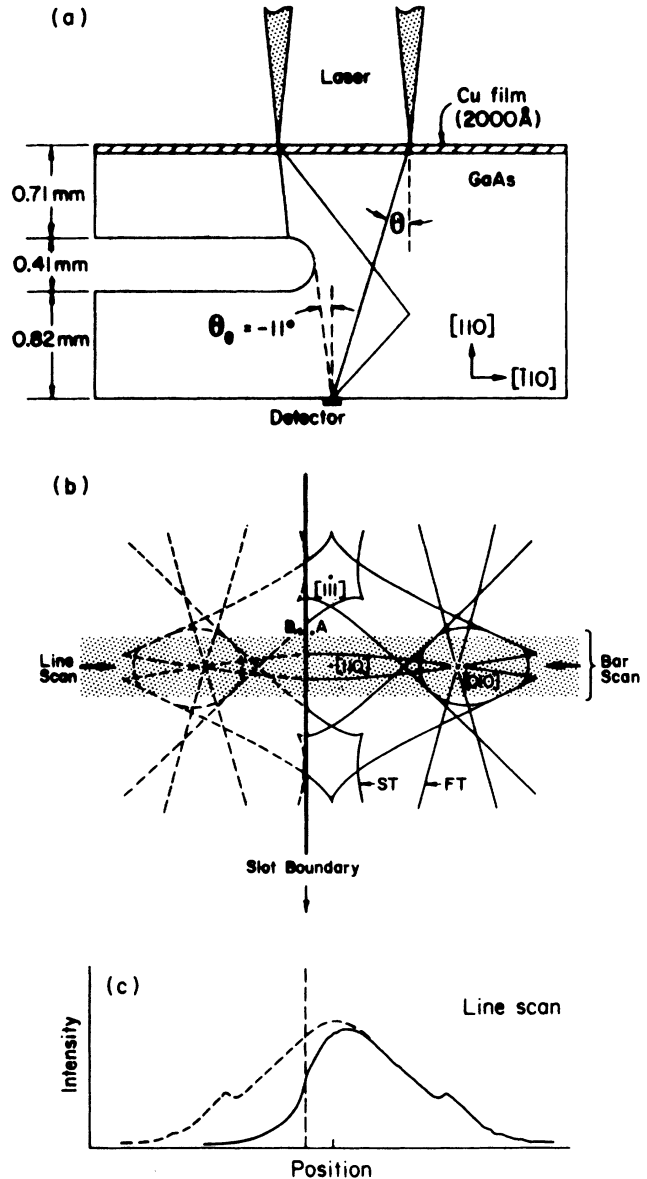


FIG. 1. (a) Schematic of the sample geometry. The angle θ_0 depends on detector placement and is determined from the observed focusing pattern. Here $\theta_0 = -11^\circ$. When the laser is at the right-hand side of the slot ($\theta > \theta_0$), ballistic and scattered phonons can reach the detector. When the laser is behind the slot ($\theta < \theta_0$), only scattered phonons can reach the detector. (b) Diagram showing the position of the slot with respect to the ballistic phonon-focusing caustics. Dashed lines indicate the position of ballistic caustics obstructed by the slot, in the region where only scattered phonons are detected. (c) Solid line is the intensity profile along the line indicated by the arrows in (b). The dashed line is the hypothetical profile if there were no slot.

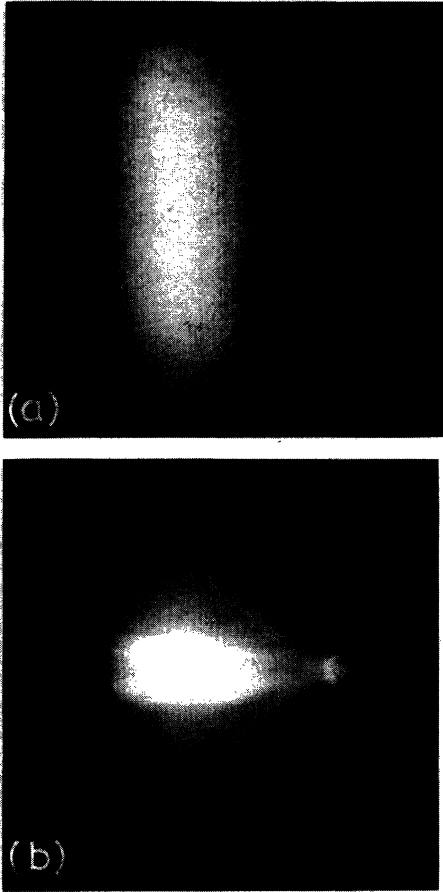


FIG. 2. (a) Experimental longitudinal (L) phonon image for the slotted crystal. The experimental time gate corresponds to $0.93t_b$ to $1.46t_b$, where t_b is the ballistic arrival time of L phonons propagating along [110]. The tunnel-junction onset frequency is 0.69 THz. (b) Experimental transverse (T) phonon image for the slotted crystal for $0.97t_b$ to $1.48t_b$, where t_b is the ballistic arrival time of T phonons propagating along [110].

outer regions of the pattern, corresponding to larger source-to-detector distances, is fairly weak due to scattering as well as the $1.5t_b$ time cutoff, with t_b referenced to the [110] direction.

Some insights are gained by observing the heat pulses in the time domain. Figure 3 contains time traces of the heat pulses for two propagation directions, labeled *A* and *B* in Fig. 1(b). The time trace *B*, “behind the slot,” shows the signal due entirely to scattered phonons. A slight translation of the laser spot to point *A* shows the ballistic signals labeled L (longitudinal) and T (transverse). Presumably, for this small translation, the scattered signal is relatively unchanged. Subtracting trace *B* from trace *A* provides the ballistic component alone at position *A*. We see that for this crystal and frequency selection ($\nu > 0.7$ THz), a large fraction of the transverse phonons reaching the detector has been scattered, i.e., the phonon mean free path is smaller than the propagation distance.

These data also indicate the difficulty one encounters in attempting to determine the mean free path or scattering rates from time traces. Precisely, what is the fraction of

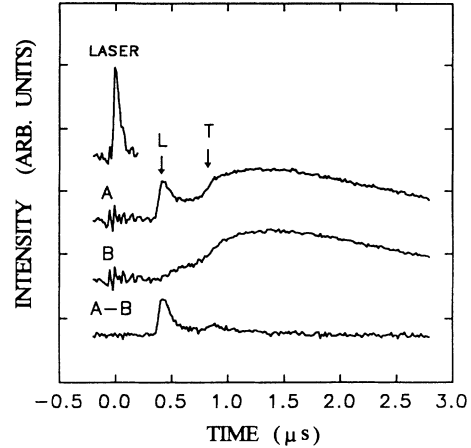


FIG. 3. Heat pulses for the slotted sample recorded by positioning the laser at points *A* and *B* shown in Fig. 1(b). Ballistic and scattered phonons are detected at *A*, but only scattered phonons are detected at *B*. The difference pulse (*A*-*B*) shows the contribution of ballistic phonons to pulse *A*. The top trace indicates the temporal position of the exciting laser pulse and the time resolution.

phonons that are scattered? From Fig. 3, one might answer that only 1% or 2% of the transverse phonons traverse the sample ballistically. However, if we had chosen points *A* and *B* to be slightly lower on the sample—say, on the strong fast-transverse (FT) focusing ridge—the ratio of ballistic to scattered flux would be much greater, perhaps by a factor of 5 or 10. To determine the phonon scattering rates, one must choose a method of comparing ballistic and scattered flux which is not so sensitive to the precise experimental conditions (e.g., choice of particular propagation direction or time window).

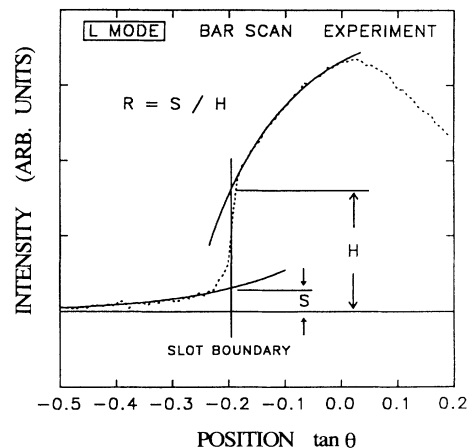


FIG. 4. Bar scan of the longitudinal phonon image shown in Fig. 2(a), corresponding to the shaded image region in Fig. 1(b) and the definition of the ledge ratio R . H is the intensity of the total phonon signal at the slot boundary, and S is the contribution of scattered phonons to H at the slot boundary. The slot boundary is not perfectly sharp so we extrapolate (solid lines) the signals (dashed line) on either side of the slot boundary to define S and H at the slot boundary.

These considerations have led us to analyzing the line or bar scans in the (110) symmetry plane, such as the data shown in Fig. 4 for the longitudinal mode. [A bar scan, which integrates over a region in y for each x position, as defined in Fig. 1(b), was chosen in this case because the scattered signals are rather weak.] The drop in intensity as one scans across the slot boundary gives a fairly well-defined measure of the scattered fraction of phonons. Shields, Tamura, and Wolfe¹⁸ found in their experiments in silicon that a "ledge ratio," $R = S/H$, where H is the intensity of the total phonon signal at the slot boundary and S is the contribution of scattered phonons to H at the slot boundary, is relatively insensitive to the selected time window or laser power. Likewise, the calculations described below show only a weak dependence on the heater temperature. The analysis procedure, then, consists of making a Monte Carlo calculation of the phonon flux for the experimental geometry for a range of scattering strengths, and determining the scattering constant which best reproduces the experimental ledge ratio. In our case, this calculation assumes a source temperature of 10 K, that only phonons with frequencies above 0.7 THz are counted, and that the scattering rate is given by the well-known form for elastic (Rayleigh) scattering valid for sub-THz phonons,^{24,25}

$$\Gamma(\nu) = A\nu^4. \quad (1)$$

The scattering constant A is treated as a variable, and is compared to the constant, $A_0 = 7.38 \times 10^{-42} \text{ s}^3$, theoretically predicted for isotope scattering in GaAs.²⁶ It should be noted that the *total* isotope-scattering rate of sub-THz phonons is independent of their propagation direction and polarization. Our calculation includes the polarization dependence of *each* scattering event, which has been shown to have a significant effect on the scattered-phonon flux.⁴

The results of this calculation for the longitudinal mode are shown in Fig. 5. The solid lines are the entire longitudinal flux, whereas the dashed lines show only the scattered component. The open circles in Fig. 6 are the ledge ratios determined from the theoretical bar scans. Also indicated on this plot is the experimentally measured ledge ratio for the longitudinal phonons, determined as in Fig. 4. We conclude that the scattering-rate constant $A = A_L$ for the longitudinal mode is $A_L = (0.8 \pm 0.5)A_0$, or alternatively $A_L \leq 1.3A_0$.

A similar analysis has been conducted for the transverse mode. Figure 7 shows a comparison between an experimental line scan and two theoretical line scans, one with $A = A_0$ and the other with $A = 4A_0$. The ledge ratios are calculated for these data, as well as for $A = 0.5A_0$ and $2A_0$, and the results are plotted in Fig. 8. The bar scan data, which include the entire "FT ridge" focusing structure [see Fig. 1(b)] are similar, with the experimental ledge ratio $R = 0.75$ and the continuum theory ranging from $R = 0.28$ at $A/A_0 = 0.5$ to $R = 0.75$ at $A/A_0 = 4.0$. We conclude that the experimental scattering rates for transverse phonons with $\nu > 0.7$ THz in our GaAs sample are approximated by the scattering-rate constant $A = A_T$, with $A_T = (4.0 \pm 0.7)A_0$.

That the scattering rates in this crystal are significantly

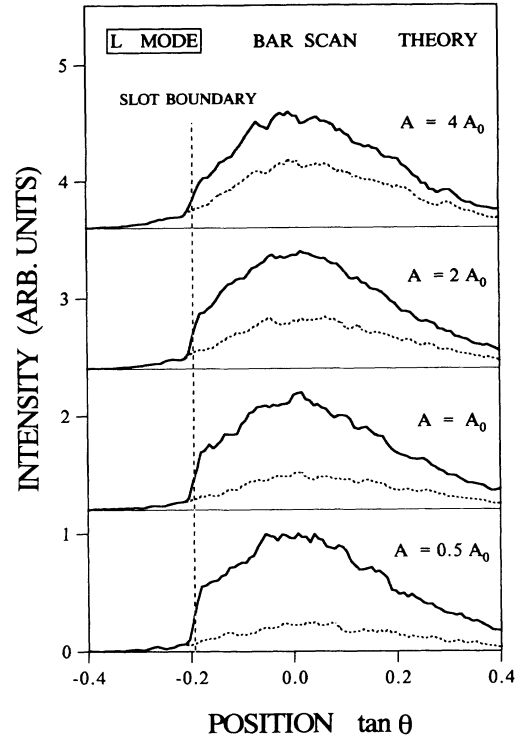


FIG. 5. Monte Carlo calculations of the bar scan for longitudinal phonons, corresponding to the experimental bar scan in Fig. 4. Bar scans are calculated for several scattering constants relative to the theoretical isotope scattering constant, A_0 . The solid lines are the entire longitudinal flux, whereas the dashed lines show only the scattered component. Note that the scattered flux is smooth across the slot boundary, implying the rise in total flux is almost entirely due to ballistic phonons.

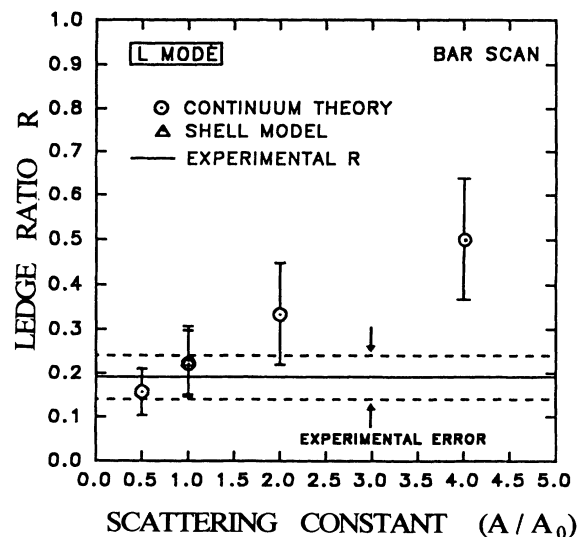


FIG. 6. Determination of the scattering constant for the longitudinal mode, using a bar scan. The ledge ratio for each calculation shown in Fig. 5 is represented as a circle. The horizontal line is the experimental value of the ledge ratio.

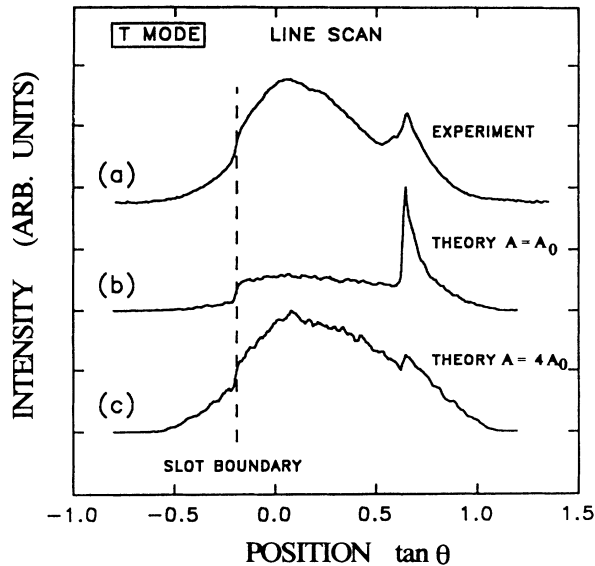


FIG. 7. (a) Experimental line scan of the intensity of the transverse mode as a function of position for the image line shown in Fig. 1(b). (b) Monte Carlo calculation corresponding to (a) for $A = A_0$. (c) Monte Carlo calculation corresponding to (a) for $A = 4A_0$.

larger than those expected for pure isotope scattering can be clearly seen from a pseudo-three-dimensional plot of the phonon flux, Fig. 9(a), which is an alternative way to display the information in the phonon image of Fig. 2(b). As indicated previously, this image is obtained for a time window between approximately t_b and $1.5t_b$. The theoretical flux distributions for $A = A_0$ and $A = 4A_0$ are plotted in Figs. 9(b) and 9(c), respectively. The scattered-phonon flux imposes a broad background on the sharper ballistic features, and the position of the slot boundary is not nearly so well defined in the $4A_0$ distri-

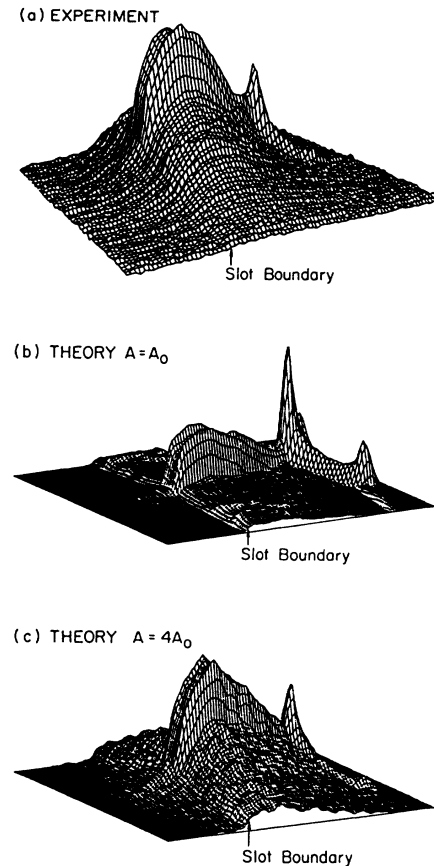


FIG. 9. (a) Pseudo-three-dimensional representation of the experimental image of the transverse mode shown in Fig. 2(b). (b) Monte Carlo image calculation for $A = A_0$. (c) Monte Carlo image calculation for $A = 4A_0$.

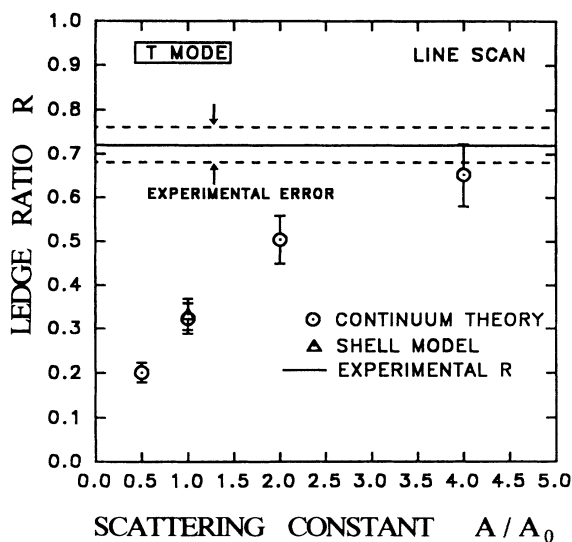


FIG. 8. Determination of the scattering constant for the transverse mode, using a line scan. The bar-scan data are similar as described in the text.

bution. The experimental data obviously resemble the $4A_0$ distribution much more closely than they do the A_0 distribution.

We conclude that the enhanced scattering rate of transverse phonons, which is clearly above that due to the intrinsic isotopic disorder, arises from defects in the crystal. The possible sources of such defects are discussed in the next section. One might ask, however, whether the ν^4 frequency dependence associated with elastic scattering from mass defects [Eq. (1)] is valid for defect scattering. The frequency dependence of the scattering rate is difficult to check with a single type of detector. Nevertheless, by changing the temperature and bias conditions, the frequency response of our tunnel-junction detector can be drastically altered. In normal operation, the sample is immersed in liquid helium at 1.6 K, and the junction is biased at a voltage less than $2\Delta/e$, where Δ is the superconducting gap and e is the charge of an electron. Ideally, only phonons with frequency greater than $2\Delta/h = 0.7$ THz are detected. The heat-pulse signal for propagation along [110], shown as the top trace in Fig. 10, contains a large component of scattered flux. If the sample is instead cooled by He vapor, and a large current bias is applied to the detector, it acts as a

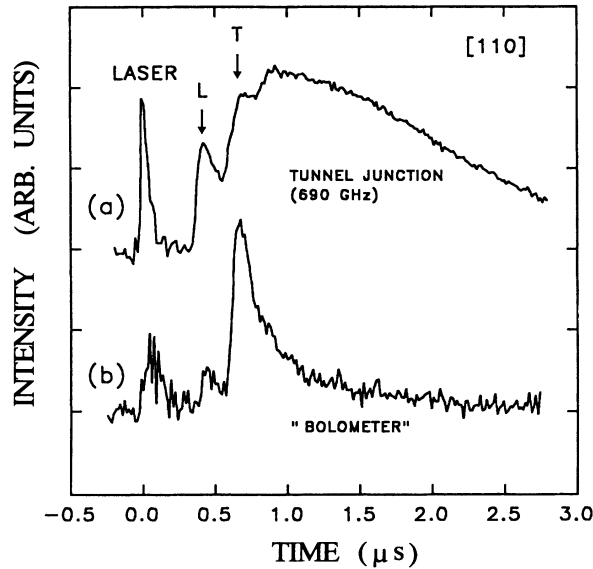


FIG. 10. Comparison of experimental heat pulses for the (a) tunnel junction and (b) "bolometer" detectors.

broadband bolometer, as indicated by a change in sign of the phonon signal. In this condition, the detector exhibits more noise, but the heat-pulse signals are observed as the bottom trace in Fig. 10. The ratio of transverse to longitudinal signal is greatly increased and the fraction of scattered phonons is greatly decreased. These observations are also reflected by much smaller ledge ratios in the "bolometer" case (not shown).

This experiment confirms that the scattering of high-frequency phonons ($\nu > 0.7$ THz) is highly mode selective, affecting the transverse phonons much more than the longitudinal phonons. The experiment also confirms that the detector used in the tunnel-junction mode is strongly selective against the lower-frequency ballistic phonons, whose actual flux at the detector, as seen in the broadband bolometer mode, is quite strong due to less scattering. The tunnel-junction mode is not only highly frequency selective but much more sensitive than the bolometer mode to phonons above 0.7 THz.

III. DISCUSSION AND CONCLUSIONS

For a diatomic lattice like GaAs, the isotope-scattering rate of long-wavelength phonons is proportional to²⁶

$$g = \frac{g_1 M_1^2 + g_2 M_2^2}{(M_1 + M_2)^2}, \quad (2)$$

and

$$g_A = \sum_{i=1}^{n_A} f_i^{(A)} \left[1 - \frac{M_i^{(A)}}{M_A} \right]^2, \quad A=1,2, \quad (3)$$

and $f_i^{(A)}$ is the fraction of i th isotope (with mass $M_i^{(A)}$) of the A th atom consisting of n_A isotopes. The average mass of the A th atom is denoted by M_A . In the case of GaAs, As is isotopically pure but Ga consists of 60.2% of

Ga⁶⁹ and 39.8% of Ga⁷¹. This leads to $g_1 = g_{\text{Ga}} = 1.97 \times 10^{-4}$ and $g_2 = g_{\text{As}} = 0$ ($M_1 = M_{\text{Ga}} = 69.72$ amu, $M_2 = M_{\text{As}} = 74.92$ amu, and mean molecular mass for GaAs is $M_{\text{GaAs}} = 144.64$ amu) and $g = 4.58 \times 10^{-5}$.

Is the excess scattering observed in these experiments due to chemical impurities substituting for Ga or As in the lattice? For such mass defects, the contribution to the elastic scattering is proportional to

$$g_I = \frac{C_I}{C_{\text{GaAs}}} \left[\frac{M_I - M_A}{M_{\text{GaAs}}} \right]^2, \quad (4)$$

where C_I and M_I are the concentration (atoms/cm³) and mass of the impurity I . Also, $C_{\text{GaAs}} = 2.21 \times 10^{22}$ molecules/cm³ and M_A are the concentration of GaAs molecules and the mass of Ga or As for which the impurity substitutes, or the mean atomic mass of GaAs for an impurity such as carbon which can substitute for either Ga or As.

A secondary-ion mass spectrometry (SIMS) analysis of our (110) sample shows that most detectable impurities are at or below the sensitivity limit of the SIMS instrument. This means $f_I = C_I / C_{\text{GaAs}} < 10^{-5}$ for $I = \text{Al, B, Be, C, Ca, Cr, Cu, F, Fe, In, K, Na, S, Se, Si, Ta, and Te}$ (in many cases f_I is much smaller). O is near the background limit of 2×10^{18} cm⁻³ ($f_I = 9 \times 10^{-5}$, $g_I = 1.4 \times 10^{-5}$). We estimate the contribution to g from all other impurities to be less than 1×10^{-5} , so the total contribution for all impurities found by the SIMS analysis is

$$g_{\text{total}} = \sum_I g_I < 2.5 \times 10^{-5}, \quad (5)$$

which is about half that for Ga isotopes. This is too small to explain the enhanced scattering of transverse phonons. Also, the total scattering rate due to mass defects should be independent of phonon polarization, but we see enhanced scattering only for transverse phonons while the scattering for longitudinal phonons is consistent with theoretical predictions.

The above treatment, however, is not applicable to the scattering of phonons by defects with symmetries lower than that of the crystal, e.g., interstitials, complex defects, or distorted substitutional impurities. Anelastic relaxation of stress fields occurs by the interaction of phonons with such defects, leading to the anisotropic and mode selective scatterings of phonons.²⁷ It is beyond the scope of this paper to discuss the effects of anelastic relaxation, but we recall the recent experiment by Culbertson *et al.*²¹ They observed that the ballistic transmission of longitudinal and transverse phonons along symmetry axes in an undoped crystal of GaAs was modified by irradiation with 1 μm light, indicating that the phonon scattering in their sample was, at least in part, due to the *EL2* defect.²² They concluded that the transverse phonons propagating along [100] were scattered by the *EL2* defect, while longitudinal phonons were unaffected. It seems plausible that such a defect, apparently present in all LEC-grown GaAs, is the source of extra transverse phonon scattering in our sample. It would be quite interesting to look for changes in the scattering rate under similar optical-excitation conditions.

ACKNOWLEDGMENTS

We would like to thank J. A. Shields and M. E. Msall for helpful discussions. We also thank J. Baker for the SIMS analysis of our sample carried out in the Center for Microanalysis of Materials in the University of Illinois MRL, which is supported by the U.S. Department of Energy under Contract No. DE-AC02-76ER01198. The support for this work was provided by the NSF grant un-

der the Materials Research Laboratory DMR89-20538. The work at Hokkaido University was supported by the Suhara Memorial Foundation and also by a Grant-in-Aid for Scientific Research from the Ministry of Education, Science and Culture of Japan (Grant No. 0155001). One of the authors (J.P.W.) wishes to thank the Japan Society for the Promotion of Science for partial support, to help complete this work.

*Present address: Advanced Micro Devices, Mail Stop 117, P.O. Box 3453, Sunnyvale, CA 94088-3453.

¹See, for example, *PHONONS 89*, edited by S. Hunklinger, W. Ludwig, and G. Weiss (World Scientific, Singapore, 1990).

²V. Narayanamurti, M. A. Chin, and R. A. Logan, *Appl. Phys. Lett.* **33**, 481 (1978).

³V. Narayanamurti, R. A. Logan, and M. A. Chin, *Phys. Rev. Lett.* **43**, 1536 (1979).

⁴M. T. Ramsbey, J. P. Wolfe, and S. Tamura, *Z. Phys. B* **73**, 167 (1988).

⁵J. A. Shields, J. P. Wolfe, and S. Tamura, *Z. Phys. B* **76**, 295 (1989).

⁶J. C. Hensel and R. C. Dynes, *Phys. Rev. Lett.* **39**, 969 (1977).

⁷J. A. Shields and J. P. Wolfe, *Z. Phys. B* **75**, 11 (1989).

⁸Y. B. Levinson, in *PHONONS 89* (Ref. 1), p. 1125.

⁹A. V. Akimov, A. A. Kaplyanskii, and E. S. Moskalenko, *Fiz. Tverd. Tela (Leningrad)* **29**, 509 (1987) [*Sov. Phys. Solid State* **29**, 288 (1987)].

¹⁰M. Greenstein, M. A. Tamor, and J. P. Wolfe, *Phys. Rev. B* **26**, 5604 (1982).

¹¹S. E. Hebboul and J. P. Wolfe, *Z. Phys. B* **73**, 437 (1989).

¹²S. E. Hebboul and J. P. Wolfe, *Z. Phys. B* **74**, 35 (1989).

¹³J. P. Wolfe, in *Festkörperprobleme (Advances in Solid State Physics)*, edited by U. Rössler (Vieweg, Braunschweig, 1989), Vol. 29, p. 75.

¹⁴G. A. Northrop and J. P. Wolfe, in *Nonequilibrium Phonon Dynamics*, edited by W. E. Bron (Plenum, New York, 1985), p. 165.

¹⁵E. Held, W. Klein, and R. P. Huebener, *Z. Phys. B* **75**, 17 (1989).

¹⁶M. Fieseler, M. Wenderoth, and R. G. Ulbrich, in *Proceedings of the 19th International Conference on the Physics of Semi-*

conductors, Warsaw, edited by W. Zawadzki (Polish Academy of Science, Warsaw, 1988), p. 1477.

¹⁷M. Fieseler, M. Schreiber, R. G. Ulbrich, M. Wenderoth, and R. Wichard, in *PHONONS 89* (Ref. 1), p. 1245.

¹⁸J. A. Shields, S. Tamura, and J. P. Wolfe, *Phys. Rev. B* **43**, 4966 (1991).

¹⁹S. Tamura, J. A. Shields, and J. P. Wolfe, *Phys. Rev. B* **44**, 3001 (1991).

²⁰B. Stock, R. G. Ulbrich, and M. Fieseler, in *Phonon Scattering in Condensed Matter*, edited by W. Eisenmenger, K. Lassmann, and S. Dottinger (Springer, Berlin, 1984), p. 97. In this paper Stock, Ulbrich, and Fieseler used a similar sample geometry to record phonon time traces, but concluded they observed 1.2-THz phonons propagating ballistically across a 1-mm-thick GaAs sample.

²¹J. C. Culbertson, U. Strom, P. B. Klein, and S. A. Wolf, *Phys. Rev. B* **29**, 7054 (1984); J. C. Culbertson, U. Strom, and S. A. Wolf, *ibid.* **36**, 2962 (1987); U. Strom, J. C. Culbertson, P. B. Klein, and S. A. Wolf, in *Proceeding of the 17th International Conference on the Physics of Semiconductors*, edited by J. D. Chadi and W. A. Harrison (Springer, Berlin, 1985), p. 1173.

²²See, for example, G. M. Martin and S. Makram-Ebeid, in *Deep Centers in Semiconductors*, edited by S. T. Pantelides (Gordon and Breach, New York, 1986), Chap. 6.

²³We thank R. G. Ulbrich for giving us this sample.

²⁴P. G. Klemens, *Proc. Phys. Soc. London, Sec. A* **68**, 1113 (1955).

²⁵P. Carruthers, *Rev. Mod. Phys.* **33**, 92 (1961).

²⁶S. Tamura, *Phys. Rev. B* **30**, 849 (1984).

²⁷A. S. Nowick and B. S. Berry, *Anelastic Relaxation in Crystalline Solids* (Academic, New York, 1972).

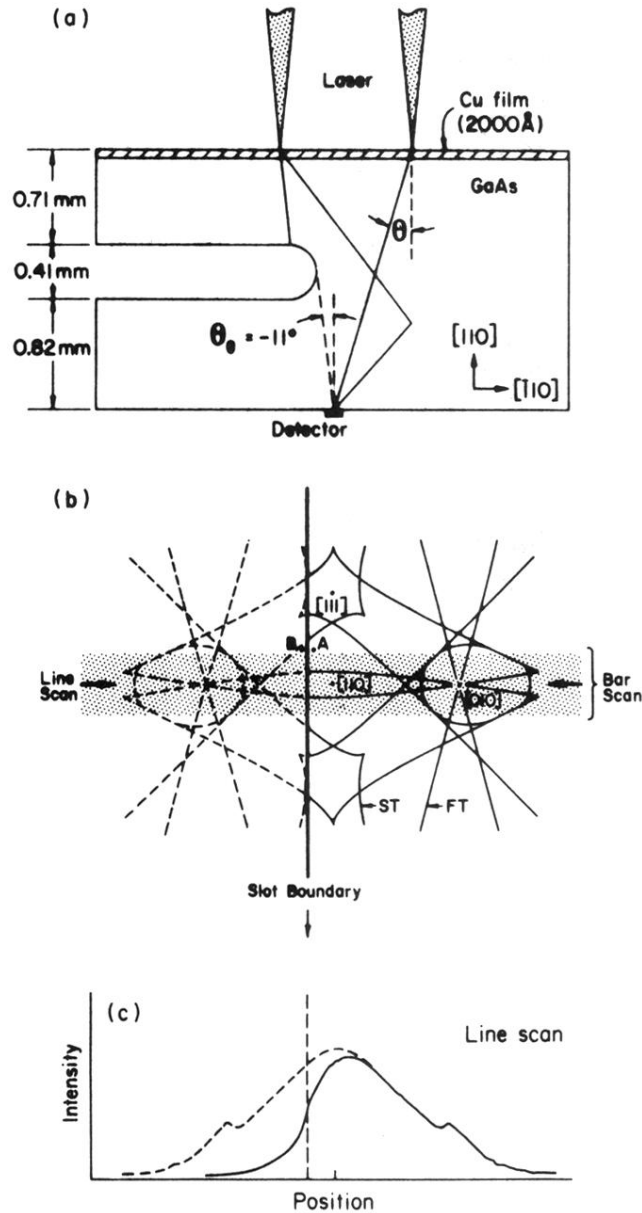


FIG. 1. (a) Schematic of the sample geometry. The angle θ_0 depends on detector placement and is determined from the observed focusing pattern. Here $\theta_0 = -11^\circ$. When the laser is at the right-hand side of the slot ($\theta > \theta_0$), ballistic and scattered phonons can reach the detector. When the laser is behind the slot ($\theta < \theta_0$), only scattered phonons can reach the detector. (b) Diagram showing the position of the slot with respect to the ballistic phonon-focusing caustics. Dashed lines indicate the position of ballistic caustics obstructed by the slot, in the region where only scattered phonons are detected. (c) Solid line is the intensity profile along the line indicated by the arrows in (b). The dashed line is the hypothetical profile if there were no slot.

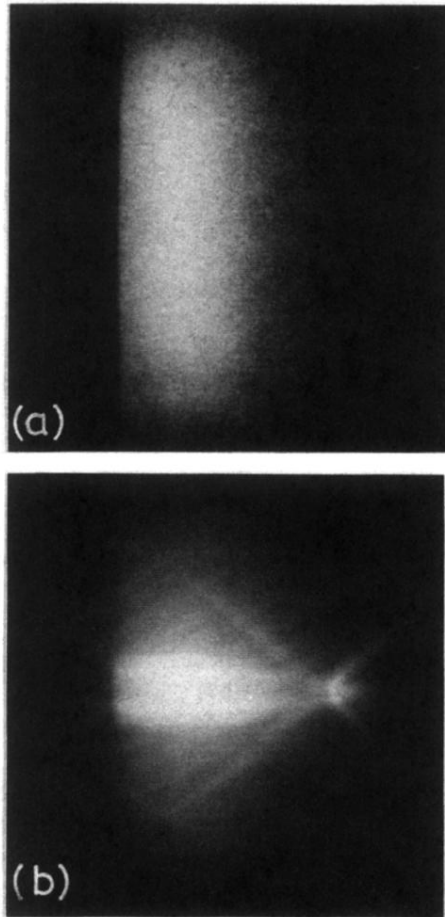


FIG. 2. (a) Experimental longitudinal (L) phonon image for the slotted crystal. The experimental time gate corresponds to $0.93t_b$ to $1.46t_b$, where t_b is the ballistic arrival time of L phonons propagating along [110]. The tunnel-junction onset frequency is 0.69 THz. (b) Experimental transverse (T) phonon image for the slotted crystal for $0.97t_b$ to $1.48t_b$, where t_b is the ballistic arrival time of T phonons propagating along [110].